Aging Cell (2012) **11,** pp683–693 Doi: 10.1111/j.1474-9726.2012.00834.x

Distinct effects of inflammation on gliosis, osmohomeostasis, and vascular integrity during amyloid beta-induced retinal degeneration

Virginie Dinet,[1,2,3]* Julien Bruban,[1,2,3]* Naima Chalour,[1,2,3] Agathe Maoui,[1,2,3] Na An,[1,2,3] Laurent Jonet,[1,2,3] Alain Buret,[1,2,3] Francine Behar-Cohen,[1,2,3] Christophe Klein,[1,2,3] Jacques Tréton[1,2,3] and Frédéric Mascarelli[1,2,3]

[1]Centre de Recherche des Cordeliers, Université Paris Descartes, UMR S 872, F-75006 Paris, France
[2]INSERM, U872, F-75006 Paris, France
[3]Université Pierre et Marie Curie – Paris6, UMRS 872, F-75006 Paris, France

Summary

In normal retinas, amyloid-β (Aβ) accumulates in the subretinal space, at the interface of the retinal pigment epithelium, and the photoreceptor outer segments. However, the molecular and cellular effects of subretinal Aβ remain inadequately elucidated. We previously showed that subretinal injection of Aβ(1–42) induces retinal inflammation, followed by photoreceptor cell death. The retinal Müller glial (RMG) cells, which are the principal retinal glial cells, are metabolically coupled to photoreceptors. Their role in the maintenance of retinal water/potassium and glutamate homeostasis makes them important players in photoreceptor survival. This study investigated the effects of subretinal Aβ(1–42) on RMG cells and of Aβ(1–42)-induced inflammation on retinal homeostasis. RMG cell gliosis (upregulation of GFAP, vimentin, and nestin) on day 1 postinjection and a proinflammatory phenotype were the first signs of retinal alteration induced by Aβ(1–42). On day 3, we detected modifications in the protein expression patterns of cyclooxygenase 2 (COX-2), glutamine synthetase (GS), Kir4.1 [the inwardly rectifying potassium (Kir) channel], and aquaporin (AQP)-4 water channels in RMG cells and of the photoreceptor-associated AQP-1. The integrity of the blood-retina barrier was compromised and retinal edema developed. Aβ(1–42) induced endoplasmic reticulum stress associated with sustained upregulation of the proapoptotic factors of the unfolded protein response and persistent photoreceptor apoptosis. Indomethacin treatment decreased inflammation and reversed the Aβ(1–42)-induced gliosis and modifications in the expression patterns of COX-2, Kir4.1, and AQP-1, but not of AQP-4 or GS. Nor did it improve edema. Our study pinpoints the adaptive response to Aβ of specific RMG cell functions.

Key words: microglia; glial cells; photoreceptors; nonsteroidal anti-inflammatory drug; blood-retina barrier; ER stress.

Correspondence
Frédéric Mascarelli, Centre de Recherche des Cordeliers, UMRS872, 15 rue de l'Ecole de Médecine, Paris 75006, France. Tel.: 00 33 1 44 27 81 80; fax: 00 33 1 44 27 81 83; e-mail: frederic.mascarelli@inserm.fr

*The first two authors contributed equally to this work and should be considered co-first authors.

Accepted for publication *7 May 2012*

Introduction

The amyloid β precursor protein (APP), together with its proteolytic fragments, plays numerous and varied roles in CNS pathology, including in Alzheimer disease (AD) (Yankner *et al.*, 1989; Selkoe, 1999). Amyloïd-β (Aβ) is deposited subretinally in normal mouse and human retinas (Hoh Kam *et al.*, 2010). With age, Aβ accumulates at the interface of the retinal pigment epithelium (RPE) and the photoreceptor outer segment tips. This finding is consistent with increased Aβ(1–42) secretion by aged human RPE cells (Glotin *et al.*, 2008). As Aβ accumulates subretinally, microglial cells in normal aged mice become bloated with cellular debris and Aβ (Hoh Kam *et al.*, 2010). The accumulation of Aβ in the subretinal space might contribute to the 25–30% reduction in photoreceptors that occurs over human lifetimes (Curcio *et al.*, 1993). We have showed that subretinal injection of Aβ(1–42) damages the RPE in young and old mice (Bruban *et al.*, 2009): photoreceptors die by apoptosis within a few days and microglial cells phagocytize photoreceptor debris and Aβ after subretinal injection of Aβ(1–42) (Bruban *et al.*, 2011). Anti-Aβ antibody immunotherapy has recently been shown to protect against RPE damage and vision loss in a mouse model of age-related macular degeneration (Ding *et al.*, 2011). The molecular processes and cellular events involved in photoreceptor cell death induced by Aβ in the subretinal space nonetheless have yet to be elucidated.

Retinal Müller glial (RMG) cells, the major glial cell types in the retina, give structural and metabolic support to photoreceptors (Bringmann *et al.*, 2006). Moreover, RMG cells are thought to influence the inner blood-retina barrier (iBRB). Impairment of the BRB is, in most cases, associated with retinal edema and subsequent vision impairment. In RMG cells, inwardly rectifying K^+ (Kir) channels and aquaporin (AQP) water channels play an important role in maintaining retinal homeostasis in normal retinas. Gliotic alterations in RMG cells under pathological conditions may contribute to edema formation and retinal degeneration (Bringmann *et al.*, 2004, 2009; Reichenbach *et al.*, 2007). Inflammation affects AQP4 and Kir4.1 expression in RMG cells of different models of retinal diseases (Bringmann & Reichenbach 2001; Bringmann *et al.*, 2006). The effects of Aβ and of Aβ-induced inflammation on RMG cell homeostasis and vascular integrity, however, have never been investigated.

In this study, we took advantage of the mouse model of subretinal injection of Aβ and showed that Aβ(1–42) induces an orderly sequence of cellular events, including apoptosis, ER stress, inflammation, gliosis, impairment of osmohomeostasis, alteration in vascular permeability, and retinal edema. These events involved microglial cells, RMG cells, vascular endothelial cells, and photoreceptors. Finally, we determined the role of inflammation in the specific reactive phenotype of RMG cells and edema during Aβ(1–42)-induced photoreceptor degeneration.

Results

Aβ induced prolonged ER stress, accompanied by sustained upregulation of the proapoptotic factors of the unfolded protein response and subsequent photoreceptor apoptosis

We compared the effects of a single subretinal injection of human Aβ (1–42) in C57BL/6J mice. A preliminary immunohistochemical study of

Aging Cell

retinal sections from Aβ(1–42)-injected mice verified that the anti-human Aβ(1–42) staining was located in the subretinal space 1 day after subretinal injection (Fig. 1A). Aβ(1–42) was still present in the subretinal space 7 days after the injection (Fig. 1B) and was detected on approximately 30% of the subretinal space surrounding the injection site through day 7 (data not shown).

Retinas in eyes injected subretinally with the inactive control Aβ(42–1) were histologically indistinguishable from those of noninjected eyes during a 7-day time period after injection (Fig. 1C). Microscopic examination of sections from the mice injected with Aβ(1–42) revealed progressive abnormalities in the retina: on day 3, retinal degeneration was at an early stage, with hypertrophic and irregularly shaped RPE (Fig. 1C, arrow). Almost all of the photoreceptor nuclei remained. There was no difference between central and peripheral retina in the degree of structural alteration (data not shown). On day 7, stretches of adjacent disorganized RPE cells, associated with the loss of photoreceptor nuclei, shortening of the inner segments (IS), and disappearance of outer segments (OS), were observed in both the central (Fig. 1D) and peripheral (Fig. 1E) parts of the Aβ(1–42)-injected retinas. On day 3 postinjection, the number of photoreceptor cell nuclei in the central and peripheral injected retinal areas did not differ significantly in the Aβ(1–42)-injected and control retinas (central retina: 10.2 ± 0.7 vs. 10.1 ± 0.5 nuclei per row; peripheral retina: 6.7 ± 0.5 vs. 6.6 ± 0.4 nuclei per row). In contrast, on day 7, we observed a 29% fall in the number of photoreceptor cell nuclei in the Aβ(1–42)-injected retinas compared with the control retinas (central retina: 7.2 ± 1.7 vs. 10.1 ± 0.5 nuclei per row, $P < 0.05$; peripheral retina: 4.7 ± 1.1 vs. 6.6 ± 0.5 nuclei per row, $P < 0.05$) (Fig. 1F), thus confirming late photoreceptor degeneration. At this stage, there was no significant difference in the number of nuclei in the ONL of Aβ(42–1)-injected retinas and the noninjected retinas (data not shown). Similarly, at the same point, the number of nuclei in the inner nuclear layer (INL) of both the central and the peripheral areas of Aβ(1–42)-injected retinas and control retinas (central retina: 6.2 ± 0.7 vs. 6.1 ± 0.5 nuclei per row; peripheral retina: 4.7 ± 0.1 vs. 4.5 ± 0.3 nuclei per row) (Fig. 1G) did not differ significantly, thereby indicating an absence of interneuron degeneration. But at this stage, the thickness of the inner retina had increased by 35–38% in Aβ(1–42)-injected retinas, compared with the control retinas (central retina: 146 ± 12 vs. 110 ± 7 μm, $P < 0.05$; peripheral retina: 98 ± 10 vs. 71 ± 4 μm, $P < 0.05$) (Fig. 1H), whereas on day 3, the Aβ(1–42)-injected retinas and control retinas had been similar in inner retinal thickness (central retina: 108.0 ± 5 vs. 113 ± 6 μm; peripheral retina: 70.1 ± 6 vs. 66 ± 7 μm). Altogether, these data indicate that Aβ(1–42) induced RPE alteration, followed by photoreceptor degeneration, and may suggest retinal edema.

Next, we investigated the processes involved in the Aβ(1–42)-induced retinal degeneration in more detail. By day 3, the detection of apoptotic cells with the TUNEL method showed no apoptotic cells in the retinas of the Aβ(42–1)-injected mice (data not shown) and very few apoptotic photoreceptors in the retinas of the Aβ(1–42)-injected mice (Fig. 2A, arrow). At this stage, the labeling intensity of the marker of autophagosomes,

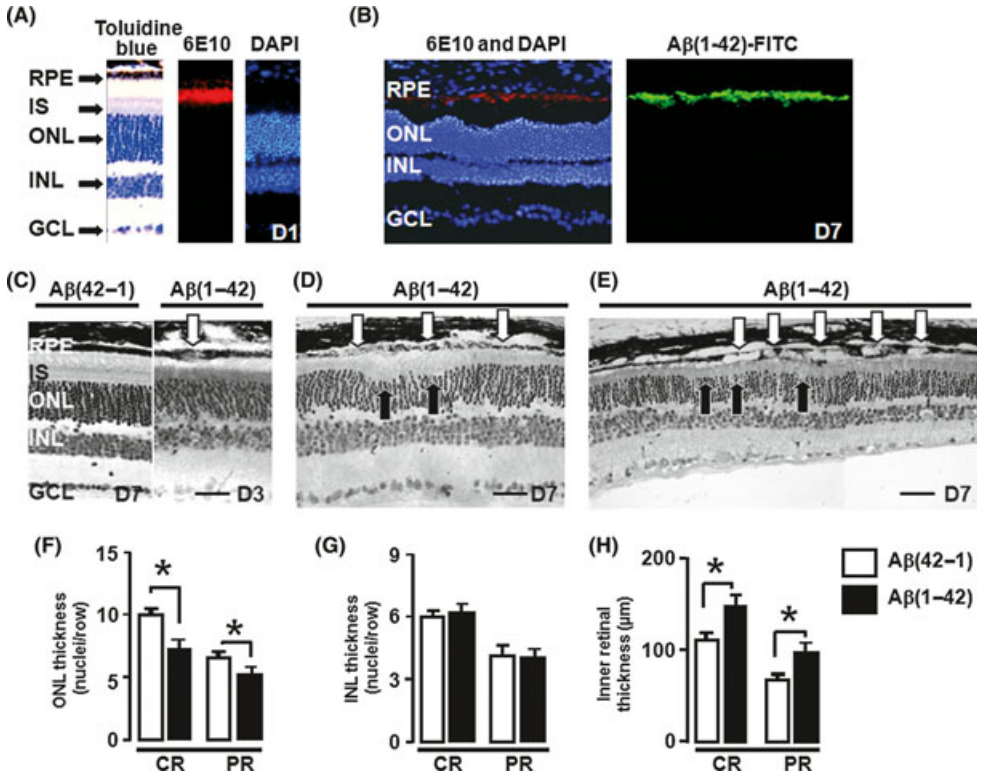

Fig. 1 Subretinal injection of Aβ in mice and its effects on retinal morphology. (A, B) Micrographs illustrating the anti-Aβ immunoreactivity of the subretinal space after injection of Aβ(1–42), with the 6E10 anti-Aβ antibody, 1 (A) and 7 (B) days after injection. (B) Comparison of the localization of anti-Aβ immunoreactivity (red fluorescence) and of injected FITC-Aβ (green fluorescence). (C–E) Micrographs of a retina section, in the center (C, D) and the periphery (E) of the retina, 3 (C) and 7 (D, E) days after injection. White arrows show abnormal RPE cells (C) associated with the loss of photoreceptor nuclei (black arrows) in the central (D) and peripheral (E) retinas after Aβ(1–42) injection. (F–H) Quantitative morphometric analysis of the thickness of the ONL (F), INL (G), and inner retina layer (H) on day 7 in the central (CR) and peripheral (PR) retinas after Aβ(1–42) injection. *$P < 0.05$. Scale bar = 50 μm. RPE, retinal pigmented epithelium; IS, inner segments; ONL, outer nuclear layer; INL, inner nuclear layer; GCL, ganglion cell layer.

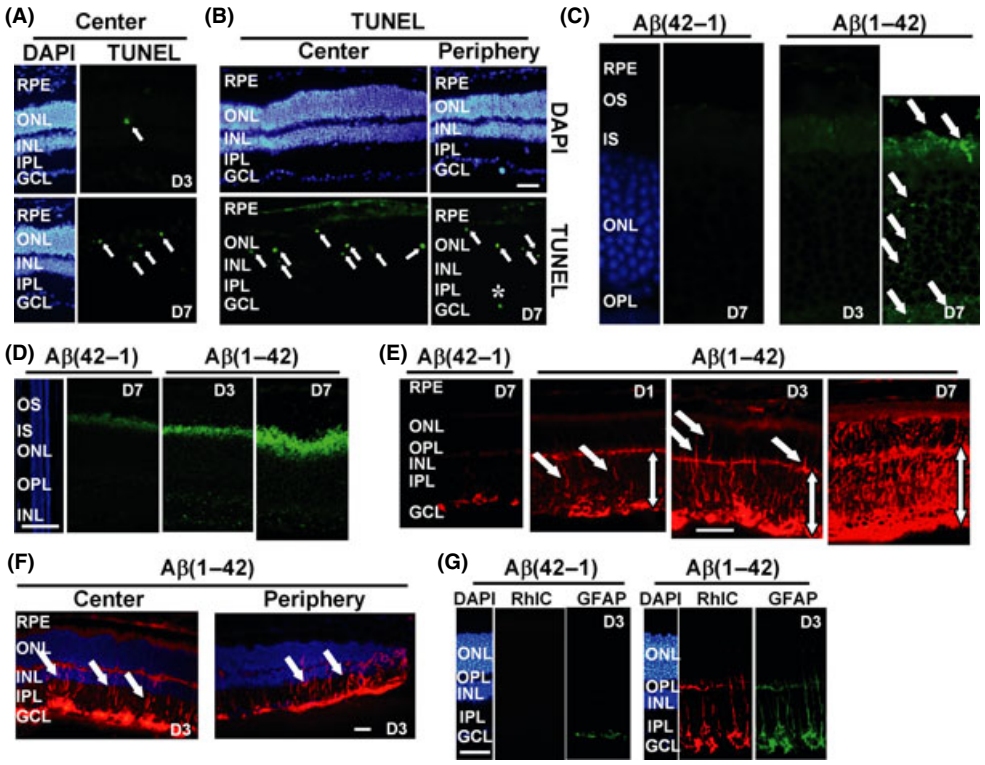

Fig. 2 Gliosis and alteration in vascular permeability preceded photoreceptor apoptosis in Aβ-injected retina. Apoptotic cells (arrows) were detected in the ONL by the TUNEL method in mice treated with Aβ(1–42) on the indicated days in the central retina (A, B) and peripheral retina (B). (C, D) Immunohistochemical analysis of the time course of expression of LC3B (C), pPERK (D), and GFAP (E) in retinal sections of mice treated with Aβ(42–1) or with Aβ(1–42) on the indicated days. (E) Oblique arrows highlight the course of GFAP expression in the retinal Müller glial (RMG) cell processes extending through the INL and ONL during retinal degeneration. Vertical double-headed arrows highlight the progressively increasing thickness of the inner retina. (F) Heterogeneity between neighboring RMG cells in the same region of the retina in respect to GFAP staining. Nuclei were counterstained with DAPI. (G) Confocal images showing the distribution of GFAP (green fluorescence) and RhIC (red fluorescence) labeling on the indicated days in the central retina. No immunoreactivity was detected when the primary antibodies were omitted (data not shown). D1: 1 day after injection; D3: 3 days after injection, D7: 7 days after injection. Magnification, ×40. Scale bar = 50 μm. RPE, retinal pigmented epithelium; IS, inner segments of photoreceptors; ONL, outer nuclear layer; OPL, outer plexiform layer; INL, inner nuclear layer; GCL, ganglion cell layer.

LC3B, in the IS increased in Aβ(1–42)-injected mice, compared with the Aβ(42–1)-injected mice (Fig. 2C). At day 3 postinjection, immunofluorescence analysis of activation of the pro-apoptotic branch of the unfolded protein response (UPR) showed weak levels of phosphorylated PERK (pPERK), distributed primarily in the IS after Aβ(42–1) injection (Fig. 2D). The intensity of the pPERK labeling in the IS increased in Aβ(1–42)-injected mice, compared with control Aβ(42–1)-injected mice (Fig. 2D). Moreover, thin punctate pPERK labeling was detected in the INL, and the ONL also showed punctate labeling for pPERK, albeit more weakly (Fig. 2D). On day 7, there were numerous apoptotic photoreceptors (Fig. 2A, arrows). At this stage, TUNEL-positive photoreceptor cell nuclei were observed in both the central and the peripheral parts of the altered retinas (Fig. 2B, arrows). Almost no TUNEL-positive cell nuclei were detected in the inner retina of Aβ(1–42)-injected mice (Fig. 2B, asterisk). At this stage, LC3B labeling in the IS was accentuated in Aβ(1–42)-injected mice, compared with control Aβ(42–1)-injected mice. Moreover, punctate LC3B labeling appeared in the IS, ONL, and OPL, consistent with the formation of autophagosomes induced by the conversion of LC3B-I to LC3B-II in photoreceptors of Aβ(1–42)-injected mice (Fig. 2C, arrows). On day 7, pPERK labeling in the IS was accentuated and appeared in the disorganized OS of Aβ(1–42)-injected mice (Fig. 2D), indicating increased activation of PERK during photoreceptor apoptosis. Consistent with these results, expression of the transcription factor CHOP was detected in the ONL of Aβ(1–42)-injected mice (data not shown).

Several studies have recently provided converging evidence for a link between photoreceptor apoptosis and ER stress by showing the upregulation of UPR- and ER-associated degradation (ERAD) genes accompanied by photoreceptor apoptosis in animal models of retinitis pigmentosa (Lin *et al.*, 2007 Gorbatyuk *et al.*, 2010; Casas-Tinto *et al.*, 2011). Moreover, the varied time courses of the individual UPR branches influence the cell's fate in response to ER stress. Therefore, we tested 28 genes known to be involved in UPR, ERAD, and autophagy by qRT-PCR analysis of Aβ(1–42)-injected retinas and control retinas at two time points, day 3 and day 7 (Table 1). Because changes in gene expression may not necessarily be associated with structural alterations in the retina after Aβ(1–42) injection, qRT-PCR analysis was performed on the entire neural retina, even though the structural alterations in the retina accounted for only approximately 30% of the retina. Analysis of the expression levels of the genes of the three branches of UPR signaling–PERK, ATF6, and IRE1–showed intense and sustained upregulation of the proapoptotic branch with increased expression of PERK (by factors of 5.1 on day 3 and 7.7 on day 7), and of CHOP and its downstream effector TRB3 (by factors of 1.9 and 2.7, respectively, on day 3) during Aβ(1–42)-induced retinal degeneration (Table 1). In contrast, a modest and transient upregulation of the prosurvival branches of the UPR was detected: XBP1 (1.7 on day 3), Bip (by a factor of 1.6 on day 3), ATF6 (by a factor of 4.4 on day 3), ERO1 (by a factor of 1.9 on day 3), and ERP72 (by a factor of 1.8 on day 3). Autophagy and ERAD are responses to ER stress, to aid cell survival and homeostasis.

Table 1 Changes in ER stress-associated gene expression accompanied the progression of retinal degeneration after Aβ injection

Gene symbol	Gene name	Change (fold) D3	Change (fold) D7
UPR			
GRP78	78 kDa glucose-regulated protein	1.6 ± 0.2*	1.3 ± 0.2
PERK	PKR-like ER kinase	5.1 ± 1.5*	7.7 ± 1.4*
ATF4	Activating transcription factor 4	1.4 ± 0.4	−1.1 ± 0.3
CHOP	C/EBP-homologous protein	1.9 ± 0.5*	1.0 ± 0.1
TRB3	Tribbles homologs 3	2.7 ± 0.7*	1.2 ± 0.3
ATF6	Activating transcription factor 6	4.4 ± 1.0*	1.6 ± 0.3*
XBP1	X-box binding	1.7 ± 0.1*	−1.7 ± 0.1*
XBP1s	Spliced form of X-box binding	4.0 ± 0.3*	1.4 ± 0.1*
HSP25	25-kDa heat shock protein	20.6 ± 4.0*	1.3 ± 0.4
HSP40	40-kDa heat shock protein	1.8 ± 0.3*	1.0 ± 0.2
HSP70	70-kDa heat shock protein	−1.2 ± 0.5	1.0 ± 0.2
ERP72	ER protein 72 kDa	1.8 ± 0.3*	1.1 ± 0.3
ERO1	ER protein endoplasmic oxidcreductin-1	1.9 ± 0.4*	−1.7 ± 0.1*
FLH	Ferritin light chain	2.0 ± 0.1*	0.8 ± 0.2
Autophagy			
ATG3	Autophagy-related 3	10.0 ± 2.0*	1.2 ± 0.2
ATG5	Autophagy-related 5	18.6 ± 3.0*	1.2 ± 0.3
BECN1/ATG6	Beclin	1.3 ± 0.5	−1.5 ± 0.1*
ATG7	Autophagy-related 7	11.9 ± 1.7*	1.2 ± 0.3
ATG8/LC3B	Light chain 3B 1	3.8 ± 0.4*	1.2 ± 0.3
ULK1	Unc-51-like kinase 1	1.6 ± 0.2*	1.2 ± 0.2
ULK2	Unc-51-like kinase 2	1.1 ± 0.3	1.5 ± 0.2*
ULK3	Unc-51-like kinase 3	1.4 ± 0.5	1.5 ± 0.2*
ERAD			
CNX	Calnexin	1.4 ± 0.1*	1.2 ± 0.2
EDEM1	ER degradation-enhancing alpha-mannosidase-like protein 1	2.3 ± 0.2*	1.2 ± 0.3
EDEM2	ER degradation-enhancing alpha-mannasidase-like protein 2	1.5 ± 0.3*	1.0 ± 0.1
EDEM3	ER degradation-enhancing alpha-mannosidase-like protein 3	1.6 ± 0.2*	1.5 ± 0.2*
UFM1	Ubiquitin fold modifier 1	2.1 ± 0.3*	1.2 ± 0.2
HRD1	ERAD-associated E3 ubiquitin-protein ligase	1.2 ± 0.2	1.0 ± 0.2

UPR, unfolded protein response.
Tests of 28 genes known to be involved in the three main processes studied during Aβ(1–42)-induced photoreceptor degeneration: unfolded protein response, autophagy, and ER-associated degradation. Their expression levels were compared in the Aβ(1–42)-injected retina and control groups, and values for fold change in expression calculated. (–) indicates lower expression in the Aβ(1–42)-injected retina group.
Data are means ± SD, $*P \leq 0.05$.

The genes coding for the autophagy-related (ATG) genes, ATG3, ATG5, ATG7, and ATG8/LC3B, was all highly but transiently upregulated (by factors of 10.0, 18.6, 11.9, and 3.8, respectively, on day 3) (Table 1). Genes coding for major proteins activating ERAD was also upregulated transiently in Aβ(1–42)-injected retinas: calnexin, EDM1, EDM2, and UFM1 (by factors of 1.4, 2.3, 1.5, and 2.1, respectively, on day 3).

Aβ induced a profound remodeling of the RMG cells, accompanied by the rupture of the iBRB

Next, we quantified changes in the expression profile of genes involved in functions of RMG, including gliosis and osmohomeostasis. Retinal Müller glial cell gliosis is characterized by the upregulation of the expression of three intermediate filament polypeptide proteins, GFAP, nestin, and vimentin (Bringmann & Reichenbach, 2001; Bringmann *et al.*, 2006). Retinal Müller glial cells mediate retinal osmohomeostasis through transcellular transport of K^+ and water, predominantly through K^+ inwardly rectifying (Kir) and AQP channels (Bringmann *et al.*, 2004). We tested nine key genes known to be involved in gliosis and retinal homeostasis by qRT-PCR analysis (Table 2). Strong and sustained upregulation of three intermediate filament proteins, GFAP (by factors of 18.4 on day 3 and 7.5 on day 7), vimentin (by factors of 7.8 on day 3 and 5.0 on day 7), and nestin (by factors of 7.5 on day 3 and 2.6 on day 7), was detected during Aβ(1–42)-induced retina degeneration (Table 2), consistent with massive and prolonged retinal gliosis. Moreover, Aβ(1–42) induced sustained upregulation of KCNJ2, encoding the inwardly rectifying K+ channel (Kir) 2.1, and AQP1, encoding the water channel AQP-1 (Table 2). Moreover, a transient upregulation of AQP4 and glial glutamate/aspartate transporter 1 (GLAST-1) was detected in Aβ(1–42)-injected mice.

Analysis of the time course of the labeling pattern of GFAP, in retinal cells by immunofluorescence, showed labeling limited to the RMG cell endfeet and astrocytes located in the ganglion cell layer (GCL) from day 1

Table 2 Transcriptional responses associated with the progression of retinal degeneration after Aβ injection include inflammation, gliosis, and deregulation of osmohomeostasis

Gane symbol	Gene name	Change (fold) D3	Change (fold) D7
Gliosis			
NES	Nestin	7.5 ± 1.4*	2.6 ± 0.3*
VIM	Vimentin	7.8 ± 1.3*	5.0 ± 0.8*
GFAP	Glial fibrillary acidic protein	18.4 ± 2.0*	7.5 ± 1.2*
Retinal homeostasis			
AQP4	Aquaporin 4	2.6 ± 0.9*	1.1 ± 0.1
AQP1	Aquaporin 1	2.7 ± 0.5*	1.6 ± 0.1*
KCNJ2	Potassium inwardly rectifying channel 2.1	4.5 ± 0.8*	3.4 ± 0.3*
KCNJ10	Potassium inwardly rectifying channel 4.1	1.4 ± 0.5	1.0 ± 0.1
EAAT-1	L-glutamate transporters GLAST-1	4.7 ± 0.7*	1.3 ± 0.1
RLBP1	Cellular retinaldehyde binding protein	1.5 ± 0.2*	1.0 ± 0.1
Inflammation			
IL1B	Interleukin 1β	5.1 ± 0.7*	3.6 ± 0.9*
IL6	Interleukin 6	8.6 ± 0.8*	5.7 ± 1.2*
IL8	Interleukin 8	9.8 ± 0.4*	2.9 ± 1.1*
INOS	Inducible NO synthase	15.3 ± 2.8*	3.1 ± 0.8*
COX2	Cyclooxygenase-2	2.7 ± 0.6*	6.4 ± 0.8*
IBA1	Ionized calcium-binding adaptor molecule 1	7.2 ± 1.4*	3.9 ± 0.3*
PPARG	Peroxisome proliferator-activated receptor γ	6.5 ± 1.5*	1.2 ± 0.5
TLR4	Toll-like receptor 4	7.0 ± 1.5*	−1.2 ± 0.5

Tests of 17 genes known to be involved in the three main processes studied during Aβ(1–42)-induced retinal degeneration: inflammation, gliosis, and retinal osmohomeostasis. These gene expression levels were compared in the Aβ(1–42)-injected retina and the control groups, and values for fold change in expression calculated. (–) indicates lower expression in the Aβ(1–42)-injected retina group.
Data are means ± SD, $*P \leq 0.05$.

to day 7 after Aβ(42–1) injection (Fig. 2E). In the Aβ(1–42)-injected mice, from day 1 onward, GFAP staining was also observed in the NFL and GCL and appeared weakly in some processes of RMG cells in the inner plexiform layer (IPL) and INL (Fig. 2E, arrows). On day 3, GFAP staining was more intense in the INL as well as in the GCL and extended to the outer plexiform layer (OPL) (Figs 2E and 3C). Rare processes of RMG cells in the OPL also stained for GFAP (Fig. 2E, arrows). From day 7, numerous RMG cell processes located in the ONL stained for GFAP (Fig. 2E, arrows and Fig. 3C). The increased portion of the inner part of the retina stained for GFAP (Fig. 2E, vertical double-headed arrows) illustrated the progressive increase in inner retinal thickness previously detected in the Aβ(1–42)-injected mice. In both the central and the peripheral retinas, we detected heterogeneity between neighboring RMG cells in the same region of the retina with respect to GFAP staining (Fig. 2F, arrows). Altogether, these data indicate that progressive RMG cell gliosis preceded photoreceptor apoptosis in the Aβ(1–42)-injected retinas.

Increase in inner retinal thickness after subretinal injection of Aβ(1–42) suggests that Aβ may affect the iBRB. The absence of abnormalities in retinal vascular permeability, illustrated by RhIC extravasation, in any of the retinal layers, indicated an intact BRB in Aβ(42–1)-injected mice (Fig. 2G). However, leakage of RhIC was observed in the inner part of the retina by day 3 after the Aβ(1–42) injection (Fig. 2G): it indicated impairment of the iBRB. The extravasated RhIC appeared to be taken up by the astrocytes and RMG cells–colocalization of RhIC labeling with GFAP staining (Fig. 2E)–and indicated alteration in vascular permeability in the neural retina of the Aβ(1–42)-injected mice.

We also used immunolabeling to study the cytoskeletal structure of RMG cells. In controls, vimentin was restricted to the RMG cell endfeet in the GCL and the entire IPL and OPL, while in Aβ(1–42)-injected mice, it was present in RMG cell processes in the INL and ONL (Fig. 3A, arrows). Beginning on day 3 after injection, we observed substantial nestin expression in the Aβ(1–42)-injected mice, most prominent in RMG cell processes that traverse the inner retina (Fig. 3B). On the other hand, it was barely detectable in control retinas.

Retinal Müller glial cells exhibit a high degree of functional and morphological polarization. We next investigated whether RMG cells expressed markers of gliosis differentially along their polarized morphology during retinal degeneration, by comparing staining for GFAP and nestin all along the RMG cells with a double-immunofluorescence approach and confocal microscopy. On day 3, the inner part of the retina (GCL, IPL, and INL) expressed almost exclusively GFAP, and the outer limiting membrane (OLM) exclusively nestin (Fig. 3C,D). At this stage, large spots costained for GFAP and nestin were detected, especially in the GCL, while only the inner part of the OPL (where rod spherules are located) costained for both (Fig. 3D, arrows). On day 7 postinjection, GFAP staining revealed thick RMG cell processes in the inner part of the retinas (Fig. 3C,E). At this stage, the distribution of GFAP and nestin had changed completely in the Aβ(1–42)-injected retina: the CGL, IPL, and the inner part of the OPL coexpressed GFAP and nestin, while the INL and ONL expressed only GFAP. Figure 3(F) illustrates alternate GFAP and nestin immunostaining all along the length of a RMG cell on day 7. These data show a dynamic and polarized redistribution of the intermediate

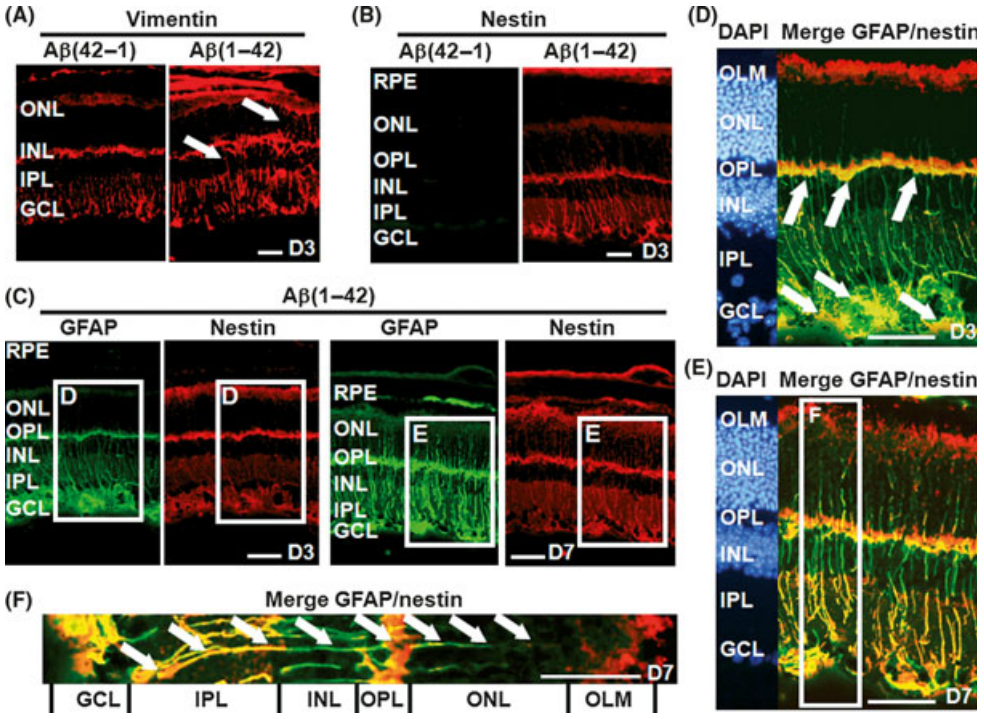

Fig. 3 Distinct polarized expression of GFAP and nestin during Aβ-induced retinal degeneration. Immunohistochemical analysis of the expression of vimentin (A), nestin (B–F), and GFAP (C–F) in retinal sections of mice treated with Aβ(42–1) or with Aβ(1–42) on the indicated days. (A) Arrows highlight vimentin expression in the retinal Müller glial (RMG) cell processes extending through the ONL and INL of Aβ(1–42)-injected retinas. (C–F) Confocal microscopy showing the expression of GFAP (green fluorescence) and nestin (red fluorescence) in Aβ(1–42)-injected retinas. (D–F) Magnification of RMG cells where colocalized labeling of GFAP and nestin can be seen. Double-labeling was created by merging the images obtained for GFAP and nestin. (D, E) Nuclei were counterstained with DAPI. (F) Magnification of RMG cells showing alternate GFAP and nestin immunostaining all along the length of a RMG cell in Aβ(1–42)-injected retinas. No immunoreactivity was detected when the primary antibodies were omitted (data not shown). Magnification, ×40. Scale bar, 50 μm. D3: 3 days after injection; D7: 7 days after injection. RPE, retinal pigmented epithelium; ONL, outer nuclear layer; OPL, outer plexiform layer; INL, inner nuclear layer; IPL, inner plexiform layer; GCL, ganglion cell layer.

filaments all along the RMG cells after Aβ(1–42) injection and thereby indicate a profound remodeling of the RMG cells as an adaptive response by the retina during photoreceptor degeneration.

Intense Aβ-induced gliosis accompanied the changed expression and redistribution of RMG cell proteins essential for retinal osmohomeostasis

To determine whether Aβ(1–42)-induced remodeling of RMG cells was associated with impairment in the localization of the proteins regulating retinal osmohomeostasis, we next studied the localization of Kir and AQP channels immunohistochemically. In control retinas, Kir4.1 was localized prominently around the blood vessels in the INL and OPL and at the inner limiting membrane (ILM) (Fig. 4A). This polarized distribution of Kir4.1 disappeared from day 3 in Aβ(1–42)-injected retinas, and Kir4.1 was uniformly distributed along the RMG cell fibers (Fig. 4A). AQP-4 in control retinas was localized predominantly in the GCL, within distinct sublayers of the IPL, around blood vessels in the GCL and INL, and in the OPL (Fig. 4B). A weak immunoreactivity for AQP-4 could be detected in the IPL, but AQP-4 immunostaining remained unchanged in the OPL and around ganglion cells and vessels in the INL by day 3 after the Aβ(1–42) injection (Fig. 4B). In control retinas, AQP-1 was predominantly observed in the outer retina (Fig. 4C). Scattered immunoreactivity for AQP-1 was also detected, albeit faintly, around the vessels, at the ILM, and in the INL. Expression of AQP-1 increased greatly throughout the neural retina by day 3 after the Aβ(1–42) injection (Fig. 4C). In control retinas, GLAST-1 was present in RMG cells from the NFL to the photoreceptor IS (Fig. 4D). The overall pattern of GLAST-1 immunostaining did not change after Aβ(1–42) injection, except for the microvilli in the OLM and IS, which were more intensely labeled on day 3 than in the control retinas (Fig. 4E). On day 3, the glutamine synthetase (GS) immunolabeling disappeared almost entirely from the retinas of Aβ(1–42)-injected mice, except for the RMG cell endfeet in the GCL (Fig. 4F). These data show mislocation and/or impairment of the polarized expression of proteins involved in retinal osmohomeostasis in RMG cells and photoreceptors before the peak of Aβ(1–42)-induced photoreceptor degeneration.

Association between inflammation and gliosis of the RMG cells in Aβ-injected retinas

Four hours after injection, microglial cells are activated and migrate to the site of injury (Bruban *et al.*, 2011). We, therefore, studied the effects of inflammation on RMG cells during Aβ(1–42)-induced retinal degeneration. First, coexpression of GFAP and F4/80 was compared in Aβ(1–42)-injected and control retinas. Retinal Müller glial and microglial cells were not activated in Aβ(42–1)-injected retinas (Fig. 5A). Increased GFAP staining was observed throughout the retinas of Aβ(1–42)-injected mice, but was particularly prominent in the areas where activated microglial cells were detected: on day 3, activated microglial cells were predominantly located in the inner part of the retina (Fig. 5B, arrowheads), and intense GFAP staining in RMG cells was observed mainly in the IPL and INL (Fig. 5B, arrows), while on day 7, activated microglial cells were located in the inner and outer parts of the retina (Fig. 5C, arrowheads) and the subretinal space, and intense GFAP staining in RMG cells was observed from the GCL to the photoreceptor IS (Fig. 5C, arrows).

Interestingly, we also detected prominent activation of RMG and microglial cells in retinal areas with no subretinal Aβ(1–42) (data not shown). We also observed dense areas of GFAP-positive RMG cell processes to the front of, but not directly in contact with, microglial cells in Aβ(1–42)-injected mice (Fig. 5D, arrows). This finding suggests that proinflammatory soluble mediators participate in RMG cell gliosis. Accordingly, we tested major genes known to be involved in inflammation by

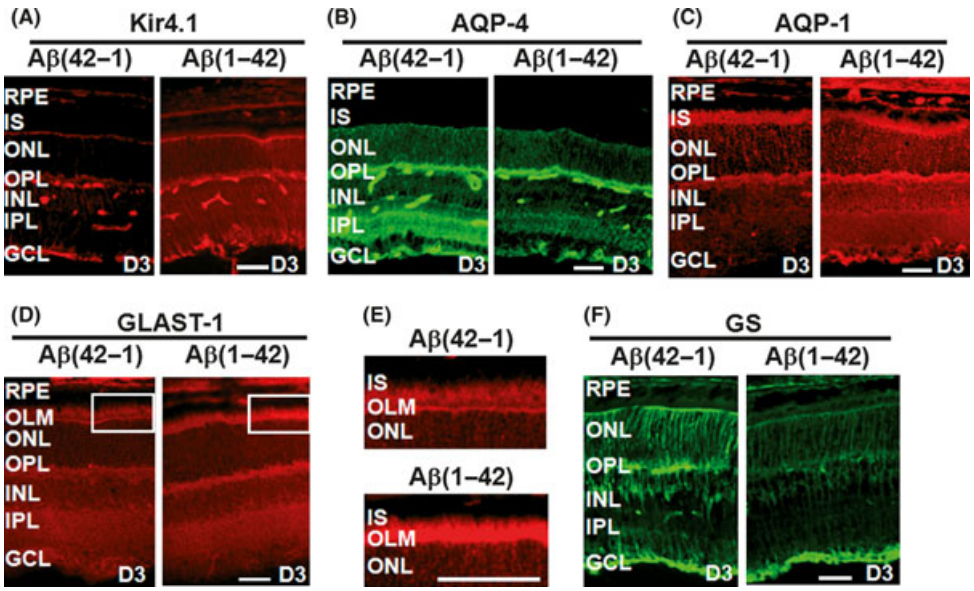

Fig. 4 Effects of Aβ on markers of glutamate, potassium, and water homeostasis during retinal degeneration. Analysis of the expression of Kir4.1 (A), AQP-4 (B), AQP-1 (C), GLAST-1 (D, E) and GS (F) by immunochemistry of the retina sections of mice treated with Aβ(42–1) or Aβ(1–42). (E) Magnification of the outer limiting membrane (OLM) and IS (white frame) shows alteration in GLAST1 expression in the Aβ(1–42)-injected retinas. Staining of Kir4.1, AQP-4, AQP-1, GLAST-1, and GS in the inactive reverse control peptide treatment group did not differ from that in the uninjected control group (data not shown). On day 1, the overall pattern of Kir4.1, AQP-4, GLAST-1, and GS immunostaining did not change in the retinas of Aβ(1–42)-injected mice in comparison with the retinas of control mice (data not shown). Magnification, ×40. Scale bar, 50 μm. No immunoreactivity was detected when the primary antibodies were omitted (data not shown). D3: 3 days after injection; D7: 7 days after injection. RPE, retinal pigmented epithelium; IS, inner segments of photoreceptors; ONL, outer nuclear layer; OPL, outer plexiform layer; INL, inner nuclear layer; IPL, inner plexiform layer; GCL, ganglion cell layer; AQP, aquaporin; GS, glutamine synthetase.

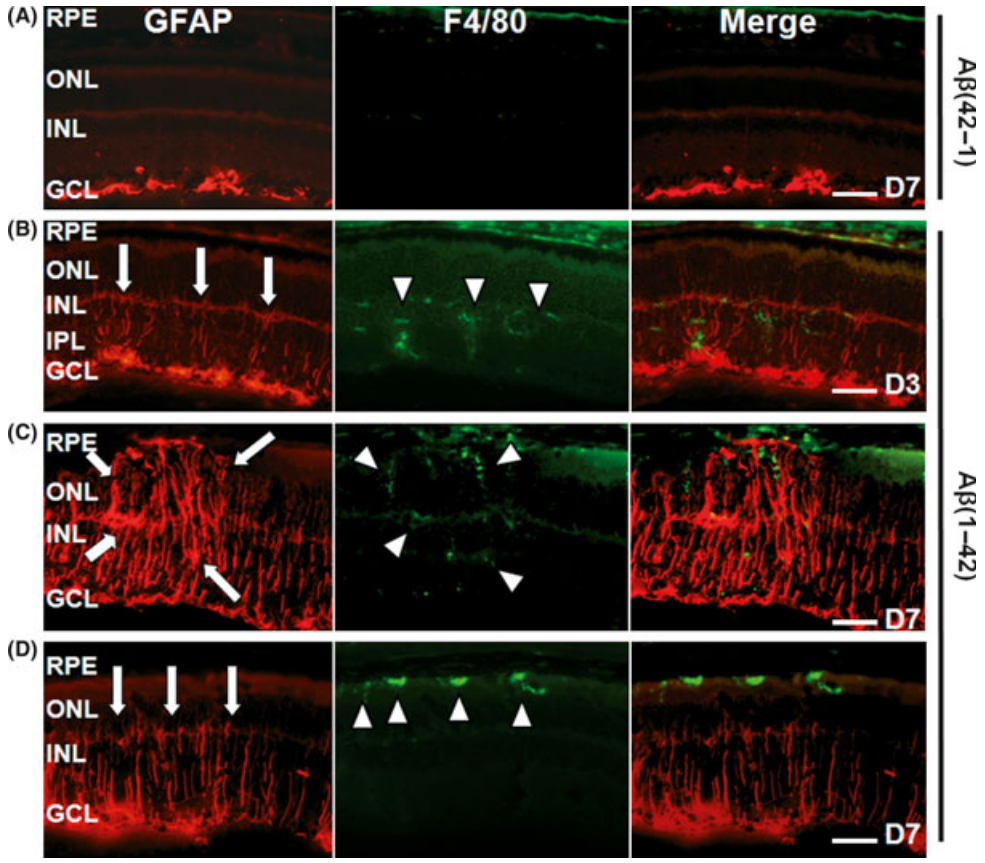

Fig. 5 Association of activated microglial cells with gliosis during Aβ-induced retinal degeneration. Immunohistochemical detection of activated microglial cells with monoclonal F4/80 antibody (green fluorescence) and GFAP-positive glial cells (red fluorescence) in the retinas injected with (A) Aβ(42–1) and (B–D) Aβ(1–42) on the indicated days. D3: 3 days after injection; D7: 7 days after injection. In B and C, arrows indicate strong activation (GFAP-positive cells) of retinal Müller glial (RMG) cells that colocalizes with activated/F4/80-positive microglial cells (arrow heads). In D, arrows indicate strong GFAP staining in the inner retina in front of activated/F4/80-positive microglial cells localized in the subretinal space (arrow heads). Double-labeling was created by merging the images obtained for F4/80 and GFAP. Magnification, ×40. Scale bar, 50 μm. No immunoreactivity was detected when the primary antibodies were omitted (data not shown). RPE, retinal pigment epithelium; ONL, outer nuclear layer; INL, inner nuclear layer; IPL, inner plexiform layer; GCL, ganglion cell layer.

qRT-PCR analysis (Table 2). Aβ(1–42) induced high and sustained upregulation of Iba1, a marker of microglial cells (by a factor of 7.2 on day 3 and of 3.9 on day 7) and of proinflammatory genes including those coding for proinflammatory cytokines (Il-1β: 5.1 and 3.6, respectively, Il-6: 8.6 and 5.7, and Il-8: 9.8 and 2.9) and cytokine-inducible iNOS (15.3 and 3.1). Expression of PPARγ, the activation of which induces COX-2 expression, was strongly upregulated (by a factor of 6.5 on day 3). Consequently, COX-2 showed strong prolonged upregulation (by a factor of 2.7 on day 3 and of 6.4 on day 7). Moreover, the expression of TLR4, a mediator of Aβ-induced neurotoxicity and inflammation, was highly upregulated (by a factor of 7.0 on day 3).

To test our hypothesis of a link between inflammation and activation of RMG cells, we investigated the effects of indomethacin, a nonselective COX-2 inhibitor and anti-inflammatory drug, on Aβ(1–42)-induced RMG cell gliosis. In Aβ(42–1)-injected retinas, COX-2 immunoreactivity was barely detectable (Fig. 6A). In contrast, intense COX-2 was induced in the RMG cells by day 3 after the Aβ(1–42) injection (Fig. 6A), confirming the strong upregulation of COX-2 detected by qRT-PCR. Pretreatment with indomethacin resulted in lower levels of COX-2 in RMG cells of Aβ(1–42)-injected mice on day 3 (Fig. 6A). Semiquantitative analysis of the immunostaining of COX-2 showed that pretreatment with indomethacin resulted in significantly less COX-2 in Aβ(1–42)-injected mice than in the animals without pretreatment (Fig. 6B). At this stage, the significantly smaller number of activated microglial cells in the retinas of the indomethacin-pretreated Aβ(1–42)-injected mice confirmed the anti-inflammatory effects of the drug (Aβ(42–1) plus indomethacin = 1.9 ± 1.0 cells per mm^2; Aβ(1–42) = 16.5 ± 1.8 cells per mm^2; Aβ(1–42) plus indomethacin = 8.8 ± 1.7 cells per mm^2, $P < 0.05$) (Fig. 6D). Retinas in eyes injected subretinally with the inactive control Aβ(42–1) contain a significant number of activated microglial cells (1.5 ± 0.8 cells per mm^2), although they were histologically indistinguishable from those of noninjected eyes during a 7-day time period after injection.

Finally, we studied the effects of indomethacin on RMG cell gliosis. The lower levels of GFAP immunolabeling in the indomethacin-pretreated Aβ(1–42)-injected mice than in the animals without pretreatment (Fig. 6B,C) demonstrated an association between inflammation and RMG cell gliosis.

Anti-inflammatory treatment partially reversed the effects of Aβ-induced impairment of retinal osmohomeostasis

To study the hypothesis that inflammation might be the cause of the modification of proteins involved in retinal osmohomeostasis during Aβ-induced retinal degeneration, we studied the effects of indomethacin

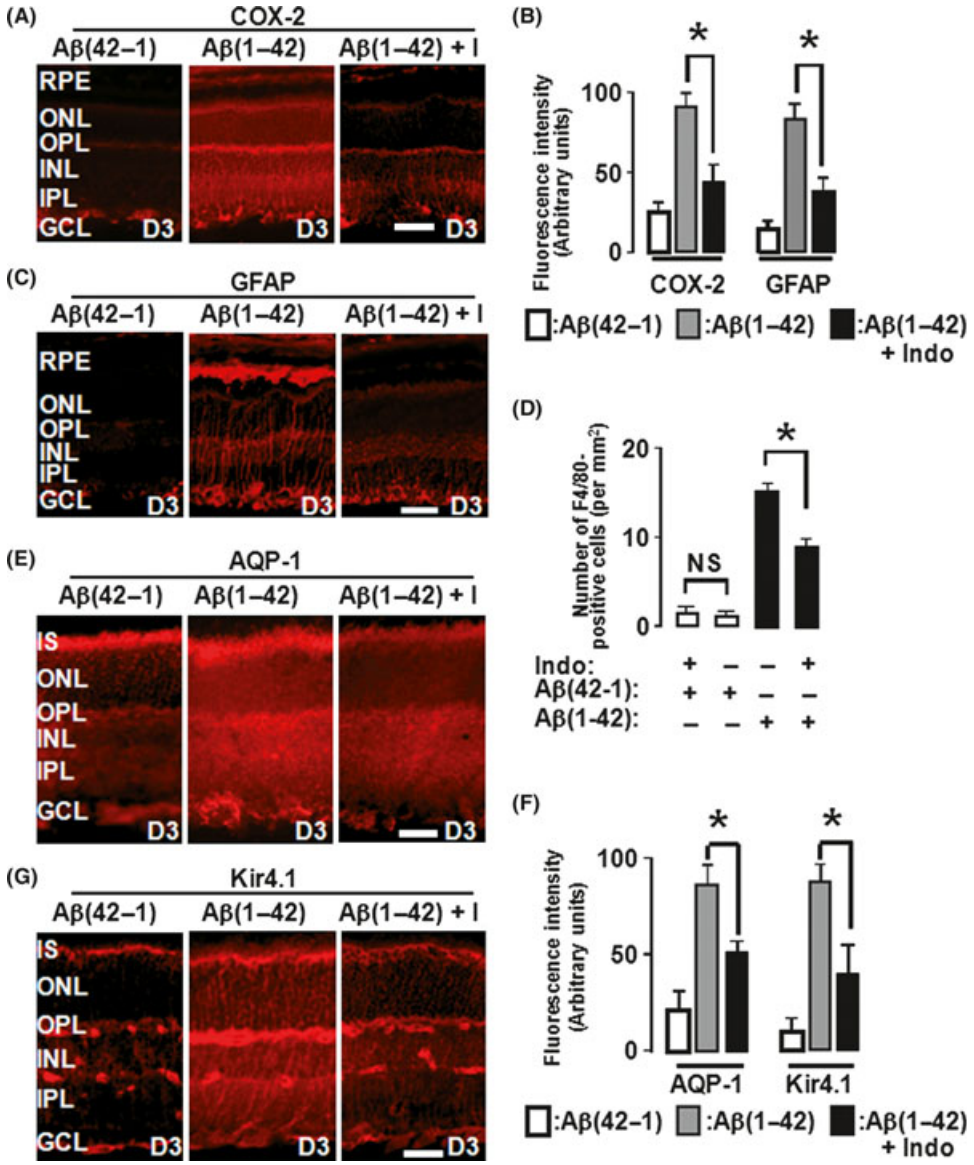

Fig. 6 Effects of indomethacin on retinal Müller glial (RMG) cells during Aβ-induced retinal degeneration. Immunohistochemical analysis on day 3 postinjection of the expression of COX-2 (A), GFAP (C), AQP-1 (E), and Kir4.1 (G) on retinal sections from mice injected with Aβ(42–1), alone; or injected with Aβ(1–42) alone; or pretreated with indomethacin (+I) and then injected with Aβ(1–42). No immunoreactivity was detected when the primary antibodies were omitted (data not shown). Magnification, ×40. Scale bar, 50 μm. (B, D, and F) Semiquantitative analysis of the relative fluorescent intensity of COX-2 (B), GFAP (B) F4/80 (D), AQP-1 (F), and kir4.1(F) immunolabeling on day 3 postinjection of retinas injected with Aβ(42–1) alone; or injected with Aβ(1–42) alone; or pretreated with indomethacin (+I) and then injected with Aβ(1–42), $*P \leq 0.05$. RPE, retinal pigmented epithelium; ONL, outer nuclear layer; OPL, outer plexiform layer; INL, inner nuclear layer; IPL, inner plexiform layer; GCL, ganglion cell layer; AQP, aquaporin.

pretreatment on the expression and localization of Kir and AQP in Aβ(1–42)-injected retinas. Analysis of AQP-1 immunolabeling showed that reduction in inflammation by indomethacin decreased the Aβ(1–42)-induced expression of AQP-1 (Fig. 6E). Similarly, reduction in inflammation reversed the increased Kir4.1 staining observed after Aβ(1–42) injection (Fig. 6G). Semiquantitative analysis of the immunostaining of Kir4.1 and AQP-1 confirmed that reduction in inflammation significantly reduced the increased expression of Kir4.1 and AQP-1 induced by Aβ(1–42) from day 3 onwards (Fig. 6F). In contrast, indomethacin treatment did not reverse the changes in immunohistochemical expression and localization of GS, AQP-4, and GLAST-1 (data not shown). Hypothetically, the repolarized expression of Kir4.1 and AQP-1 owing to indomethacin pretreatment in the Aβ(1–42)-injected retinas might also play a protective role against the retinal swelling. To test this possibility, we investigated the effects of indomethacin on the formation of retinal edema. Quantitative morphometric analysis of the inner retinal thickness in indomethacin-pretreated Aβ(1–42)-injected mice and Aβ(1–42)-injected mice showed no obvious differences in retinal swelling in the 7 days after pretreatment (central retina: 146 ± 12 vs. 154 ± 11 μm; peripheral retina: 98 ± 10 vs. 95 ± 8 μm), indicating that edema did not improve after indomethacin pretreatment.

Discussion

The retinal adaptive response to Aβ-induced lethal ER stress takes place in an integrated multicellular system

We showed that RMG cell activation is one of the earliest signs observed in the neural retina after subretinal injection of Aβ. The simultaneous dynamic and complex polarized redistribution of the intermediate filaments, GFAP, vimentin, and nestin, all along the RMG cells during Aβ-induced photoreceptor degeneration, demonstrates remodeling of the RMG cells in response to Aβ. The long-term changes in the expression/localization of Kir and AQP channels suggest that Aβ durably affects retinal osmohomeostasis in these mice, consistent with sustained edema. Only Aβ-induced activation of microglial cells precedes gliosis, which is then followed by compromised iBRB, edema, and photoreceptor degeneration. Altogether, our data are consistent with a model (Fig. S3, Supporting information) in which Aβ induces a very orderly sequence of molecular and cellular events, involving microglial cells, RMG cells, vascular endothelial cells, and photoreceptors. Prolonged photoreceptor cell apoptosis may be explained by the transient activation of the antiapoptotic responses of the retina to ER stress, including UPR, ERAD, and autophagy, and the sustained activation of the proapoptotic branch of the UPR, combined with prolonged inflammation and gliosis. In the P23H rat model of photoreceptor degeneration (Lin *et al.*, 2007), persistent ER stress-induced photoreceptor degeneration, together with transient upregulation of Bip and transient activation of IRE1 signaling, is consistent with transient upregulation of Bip and transient upregulation of XBP1s during Aβ-induced photoreceptor degeneration. Extended upregulation of PERK, the proapoptotic branch of the UPR, associated with extended pPERK levels in photoreceptors, confirms prolonged ER stress in Aβ-injected retinas. Sustained pPERK levels have also been observed throughout photoreceptor degeneration in P23H rats (Lin *et al.*, 2007).

Role of inflammation in the subretinal Aβ-induced RMG cell gliosis

Retinal edema did not improve after indomethacin pretreatment in Aβ-injected mice. This result was quite surprising given that the inhibition of COX prevents the osmotic swelling of RMG cells in pathologically altered retinas (Uckermann *et al.*, 2005; Pannicke *et al.*, 2006). It suggests that preventing Aβ-induced mislocalization of Kir4.1 and AQP-1 by indomethacin was not sufficient to reduce edema. We can thus speculate that Aβ may impair retinal osmohomeostasis by altering other water channels expressed by either the RPE or the RMG cells. During the preparation of this manuscript, expression of AQP-0, 3, 5, 6, 8, 9, 11, and 12 has been identified in the neural retinas and the RPE (Hollborn *et al.*, 2011). We cannot rule out the possibility that Aβ also affects the expression/distribution of these water channels after subretinal injection. A second hypothesis is that another process is involved in RMG cell gliosis. Inflammation and oxidative stress are known to be involved in retinal edema. We previously detected massive oxidative stress in the retina of Aβ-injected mice (Bruban *et al.*, 2011). Therefore, we cannot rule out the hypothesis that oxidative stress co-induces RMG cell impairment.

Although we detected the upregulation of IL-1β, IL-6, and IL-8 in the neural retina of Aβ(1–42)-injected mice, we cannot rule out the possibility that RPE plays a role in the Aβ-induced inflammation. A microarray identified the production of Il-1β and Il-8 as the main response to Aβ(1–40) of RPE cells in culture (Kurji *et al.*, 2010). Therefore, RPE may be a major source of inflammation after Aβ injection. The RPE may also play a role in the migration of microglial cells to the subretinal space of Aβ(1–42)-injected mice, because Aβ(1–40) stimulates the production of CCL2 and Il-8, by RPE cells in culture (Wang *et al.*, 2009; Kurji *et al.*, 2010). This might suggest that microglial cells are recruited by CCL2 and/or Il-8 produced by RPE cells. But the upregulation of CCL2 and Il-8 in Aβ(1–42)-injected mice was detected in the neural retina devoid of RPE cells (Bruban *et al.*, 2011). This finding indicates that cells of the neural retina are also able to produce CCL2 and Il-8 in the presence of Aβ. Under pathological conditions, RMG cells produce CCL2, as well as IL-8 (Yoshida *et al.*, 2004; Goczalik *et al.*, 2008). Retinal Müller glial cell-derived CCL2 and/or IL-8 may therefore participate in the development of retinal inflammation.

In conclusion, our study indicates that inflammation mediates a part but not all of the specific RMG cell gliotic response to Aβ-mediated ER stress during photoreceptor degeneration. The similarities of the pathogenic pathways between some retinal degenerative diseases and AD suggest that studying the link between inflammation, retinal osmohomeostasis, and APP processing during retinal degeneration may have significant applications in the treatment of these retinal diseases.

Experimental procedures

Animals and animal treatment

Twelve-month-old C57BL/6 mice (Janvier, Le Genest Saint Isle, France) were used. All procedures involving mice conformed to the resolution on the use of animals in research of the Association for Research in Vision and Ophthalmology and to the guidelines of the Institut National de la Santé et de la Recherche Médicale Committee on Animal Research.

To investigate the effects of Aβ(1–42) on the retina, mice were anesthetized with sodium pentobarbital (5 mg/100 g) and underwent a single unilateral subretinal injection with Aβ peptide (1.25 nmol/2 μL) in PBS, as previously described (Bruban *et al.*, 2009, 2011). Fluorescein isothiocyanate (FITC)-conjugated Aβ(1–42) and its inactive reverse control peptide, Aβ(42–1), were supplied by Bachem (Weil am Rhein, Germany). The Aβ peptides were prepared by suspending lyophilized preparations of Aβ in autoclaved 0.22-μm-filtered Milli Q water (500 μM) just before use and then rotating the solutions slowly at 37 °C for 5 days with a rotating cultivator, as previously described (Bruban *et al.*, 2011; Hoshi *et al.*, 2003; Walsh *et al.*, 2002; Zhang *et al.*, 2003, and technical notes by Bachem).

The effects of indomethacin were investigated after topical administration of Indocollyre (0.1% indomethacin; Bausch & Lomb, Montpellier, France) to the eye. Mice were treated with one drop, four times a day, 1 day before subretinal injection of Aβ and for the next 7 days.

Assessment of vascular permeability

Vascular permeability is identified by rhodamine isothiocyanate (RhIC) leakage. In normal retinas with an intact BRB, this dye diffuses freely through the choriocapillaries and Bruch's membrane, but does not diffuse through the tight junctions of the RPE and the retinal vascular endothelium. Control and Aβ(1–42)-injected mice were given an intraperitoneal injection of RhIC (5 μL 1% RhIC per g body weight) dissolved in normal saline, either 2 or 6 days after subretinal injection, and then sacrificed 24 h later. The eyes were then removed and frozen retinal sections cut and processed, as described earlier. Immunofluorescence labeling using GFAP antibody followed the method described previously for double-immunofluorescence labeling. Cellular colocalization was then studied by confocal microscopy.

Retinal immunohistochemistry

Eye balls were harvested from mice at days 1, 3, and 7 postinjection. The injection site and orientation of the eye were identified. The eyes were dissected along the vertical meridian, their lenses removed, and the eye posterior hemispheres were prepared for frozen sections (12 μm). Post-fixed tissue sections were saturated with 1% BSA and 1% normal goat serum in PBS and permeabilized in 0.1% Triton X-100. The sections were then incubated overnight with the primary antibodies. After washing, sections were incubated in a solution of 1:100 of secondary rat anti-mouse antibody conjugated to Alexa red, goat anti-rabbit antibody conjugated to Alexa green, and goat anti-rat antibody conjugated to Alexa red, (Invitrogen, Cergy-Pontoise, France) for 60 min. The slides were then stained for 5 min with DAPI. Primary antibodies were those to rat monoclonal anti-F4/80 (1:100; Serotec, Colmar, France), mouse monoclonal anti-human Aβ (1:500, 6E10; Calbiochem, Molsheim, France), anti-vimentin (1:100; Abcam, Paris, France), anti-glutamine synthetase (1:200; Millipore, Molsheim, France), rabbit polyclonal anti-GFAP (1:200; Dako, Trappes, France), anti-Kir4.1 (1:200; Alomone Laboratories, Jerusalem, Israel), anti-aquaporin (AQP)-1 (1:100; Sigma, Lyon, France), and anti AQP-4 (1:100; Sigma). As a control, the primary antibody was omitted: no staining was observed in any control. At least six mice were used at each selected treatment time. Immunochemistry data were semiquantitatively analyzed with ImageJ analysis software (National Institutes of Health) as previously described (Bruban *et al.*, 2011). Signal intensity for each mouse was measured on nonoverlapping fields of 300 μm of linear retinal length. To compare results from different mice, the mean of the ratio between fluorescent signal values and background was calculated first for each animal ($n = 3$) and then the mean for five animals with six sections per retina. Each data point was the mean ± SD. Some of the sections were processed with historesin and stained with toluidine blue to reveal the retinal structure. Sections were analyzed by microscopy with a Leica Aristoplan (Leica, Paris, France) and photographed with a Spot camera (Optilas, Evry, France). Exposure parameters were identical for all samples.

Quantitative real-time polymerase chain reaction (qRT-PCR)

The eyes were enucleated, retinas were removed at days 3 and 7 postinjection, and the RPE was dissected away under a binocular microscope, with fine forceps. Neural retina samples from three animals were pooled for each condition Aβ(42–1) and Aβ(1–42). The isolation of neural retina from RPE was confirmed by the failure to detect expression of RDH5, LRAT, and RPE65 in the neural retina preparations after 35 PCR cycles in RT-PCR analysis. Total RNA neural retina was isolated with TRIZOL reagent (Invitrogen) according to the manufacturer's instructions, and SuperScript II Reverse Transcriptase (Invitrogen) was used to reverse transcribe 2 μg of mRNA. Amplification reaction assays contained 1× SYBR Green PCR Mastermix (Applied Biosystems, Saint Aubin, France). All real-time PCR oligonucleotide primers had previously been validated experimentally by QPCR, agarose gel analysis, sequencing, and BLAST. The PCR primer sequences used shown in Fig. S2 (Supporting information). A hot start at 95 °C for 5 min was followed by 40 cycles at 95 °C for 15 s and 60 °C for 1 min with the 7300 SDS thermal cycler (Applied Biosystems). Controls with no reverse transcriptase were run for each assay to confirm the absence of genomic DNA contamination. Control qRT-PCRs were performed without cDNA templates. The standard curve method (Prism 7700 Sequence Detection System, Applied Biosystems, Saint Aubin, France; ABI User Bulletin number 2) was used for relative quantification of gene expression. At least two experiments were conducted for each gene and each retina sample. At each experiment, each individual sample was run in triplicate wells and the C_t value for each well was recorded at the end of the reaction. The average and standard deviation of the three C_t values were calculated. Gene expression levels were normalized to GAPDH for each retinal tissue sample and calculated relative to normal retinal tissue (control) with the following equation: relative expression $= 2^{-(\text{sample}\Delta C_t - \text{control}\Delta C_t)}$ where ΔC_t = mean C_t(target)–mean C_t(GAPDH).

Statistical analyses

Statistical analyses were performed by computer (GraphPAD Software Inc, La jolla, CA, USA). Normality was assessed with the Kolmogorov–Smirnov test. Differences between groups were compared with the non-parametric Kruskal–Wallis test, and paired comparisons between groups used the Mann–Whitney test. Data are expressed as means ± SD.

Acknowledgments

This study was supported by the Fédération des Aveugles et Handicapés Visuels de France (NA), the Ministère de la Recherche (JB, NC and AM), and the Agence Nationale de la Recherche Scientifique (ANR) (FM and VD). We thank Jo Ann Cahn for editorial assistance. Disclosure Statement: None of the authors of this paper has any potential or actual financial interests or conflict of interest.

Author contributions

Frédéric Mascarelli designed and organized this study, carried out the data analysis, wrote the manuscript, and was responsible for the study. Virginie Dinet and Julien Bruban performed the largest part of the study, and carried out data analysis and writing. Naima Chalour and Agathe Maoui participated to Q-PCR experiments, Laurent Jonet contributed to the immunochemistry experiments, Alain Buret participated in animal care, Francine Behar-Cohen carried out animal injections, Christophe Klein participated in image processing, and Jacques Tréton participated in the discussion and interpretation of the final results.

References

Bringmann A, Reichenbach A (2001) Role of Muller cells in retinal degenerations. *Front. Biosci.* **6**, 72–92.

Bringmann A, Reichenbach A, Wiedemann P (2004) Pathomechanisms of cystoids macular edema. *Ophthalmic Res.* **36**, 241–249.

Bringmann A, Pannicke T, Grosche J, Francke M, Wiedemann P, Skatchkov SN, Osborne NN, Reichenbach A. (2006) Muller cells in the healthy and diseased retina. *Prog. Retin. Eye Res.* **25**, 397–424.

Bringmann A, Iandiev I, Pannicke T, Wurm A, Hollborn M, Wiedemann P, Osborne NN, Reichenbach A. (2009) Cellular signaling and factors involved in Muller cell gliosis: neuroprotective and detrimental effects. *Prog. Retin. Eye Res.* **28**, 423–451.

Bruban J, Glotin AL, Dinet V, Chalour N, Sennlaub F, Jonet L, An N, Faussat AM, Mascarelli F. (2009) Amyloid-beta(1–42) alters structure and function of retinal pigmented epithelial cells. *Aging Cell* **8**, 162–177.

Bruban J, Maoui A, Chalour N, An N, Jonet L, Feumi C, Tréton J, Sennlaub F, Behar-Cohen F, Mascarelli F, Dinet V. (2011) CCL2/CCR2-mediated inflammation protects photoreceptor from Aβ-induced apoptosis. *Neurobiol. Dis.* **42**, 55–72.

Casas-Tinto S, Zhang Y, Sanchez-Garcia J, Gomez-Velazquez M, Rincon-Limas DE, Fernandez-Funez P (2011) The ER stress factor XBP1s prevents amyloid-beta neurotoxicity. *Hum. Mol. Genet.* **20**, 2144–2160.

Curcio CA, Millican CL, Allen KA, Kalina RE (1993) Aging of the human photoreceptor mosaic: evidence for selective vulnerability of rods in central retina. *Invest. Ophthalmol. Vis. Sci.* **34**, 3278–3296.

Ding JD, Johnson LV, Herrmann R, Farsiu S, Smith SG, Groelle M, Mace BE, Sullivan P, Jamison JA, Kelly U, Harrabi O, Bollini SS, Dilley J, Kobayashi D, Kuang B, Li W, Pons J, Lin JC, Bowes Rickman C (2011) Anti-amyloid therapy protects against retinal pigmented epithelium damage and vision loss in a model of age-related macular degeneration. *Proc. Natl Acad. Sci. USA* **108**, E279–E287.

Glotin AL, Debacq-Chainiaux F, Brossas JY, Faussat AM, Tréton J, Zubielewicz A, Toussaint O, Mascarelli F (2008) Prematurely senescent ARPE-19 cells display features of age-related macular degeneration. *Free Radic. Biol. Med.* **44**, 1348–1361.

Goczalik I, Ulbricht E, Hollborn M, Raap M, Uhlmann S, Weick M, Pannicke T, Wiedemann P, Bringmann A, Reichenbach A, Francke M (2008) Expression of CXCL8, CXCR1, and CXCR2 in neurons and glial cells of the human and rabbit retina. *Invest. Ophthalmol. Vis. Sci.* **49**, 4578–4589.

Gorbatyuk MS, Knox T, LaVail MM, Gorbatyuk OS, Noorwez SM, Hauswirth WW, Lin JH, Muzyczka N, Lewin AS (2010) Restoration of visual function in P23H rhodopsin transgenic rats by gene delivery of BiP/Grp78. *Proc. Natl Acad. Sci. USA* **107**, 5961–5966.

Hoh Kam J, Lenassi E, Jeffery G (2010) Viewing ageing eyes: diverse sites of amyloid Beta accumulation in the ageing mouse retina and the up-regulation of macrophages. *PLoS ONE* **5**, e13127.

Hollborn M, Dukic-Stefanovic S, Pannicke T, Ulbricht E, Reichenbach A, Wiedemann P, Bringmann A, Kohen L (2011) Expression of aquaporins in the retina of diabetic rats. *Curr. Eye Res.* **36**, 850–856.

Hoshi M, Sato M, Matsumoto S, Noguchi A, Yasutake K, Yoshida N, Sato K (2003) Spherical aggregates of beta-amyloid (amylospheroid) show high neurotoxicity and activate tau protein kinase I/glycogen synthase kinase-3beta. *Proc. Natl Acad. Sci. USA* **100**, 6370–6375.

Kurji KH, Cui JZ, Lin T, Harriman D, Prasad SS, Kojic L, Matsubara JA (2010) Microarray analysis identifies changes in inflammatory gene expression in response to amyloid-beta stimulation of cultured human retinal pigment epithelial cells. *Invest. Ophthalmol. Vis. Sci.* **51**, 1151–1163.

Lin JH, Li H, Yasumura D, Cohen HR, Zhang C, Panning B, Shokat KM, Lavail MM, Walter P (2007) IRE1 signaling affects cell fate during the unfolded protein response. *Science* **318**, 944–949.

Pannicke T, Iandiev I, Wurm A, Uckermann O, vom Hagen F, Reichenbach A, Wiedemann P, Hammes HP, Bringmann A (2006) Diabetes alters osmotic swelling characteristics and membrane conductance of glial cells in rat retina. *Diabetes* **55**, 633–639.

Reichenbach A, Wurm A, Pannicke T, Iandiev I, Wiedemann P, Bringmann A (2007) Müller cells as players in retinal degeneration and edema. *Graefes Arch. Clin. Exp. Ophthalmol.* **245**, 627–636.

Selkoe DJ (1999) Translating cell biology into therapeutic advances in Alzheimer's disease. *Nature* **399**, 23–31.

Uckermann O, Kutzera F, Wolf A, Pannicke T, Reichenbach A, Wiedemann P, Wolf S, Bringmann A (2005) The glucocorticoid triamcinolone acetonide inhibits osmotic swelling of retinal glial cells via stimulation of endogenous adenosine signaling. *J. Pharmacol. Exp. Ther.* **315**, 1036–1045.

Walsh DT, Montero RM, Bresciani LG, Jen AY, Leclercq PD, Saunders D, EL-Amir AN, Gbadamoshi L, Gentleman SM, Jen LS (2002) Amyloid-beta peptide is toxic to neurons in vivo via indirect mechanisms. *Neurobiol. Dis.* **10**, 20–27.

Wang J, Ohno-Matsui K, Yoshida T, Shimada N, Ichinose S, Sato T, Mochizuki M, Morita I (2009) Amyloid-beta up-regulates complement factor B in retinal pigment epithelial cells through cytokines released from recruited macrophages/microglia: another mechanism of complement activation in age-related macular degeneration. *J. Cell. Physiol.* **220**, 119–128.

Yankner BA, Dawes LR, Fisher S, Villa-Komaroff L, Oster-Granite ML, Neve RL (1989) Neurotoxicity of a fragment of the amyloid precursor associated with Alzheimer's disease. *Science* **245**, 417–420.

Yoshida S, Yoshida A, Ishibashi T (2004) Induction of IL-8, MCP-1, and bFGF by TNF-alpha in retinal glial cells: implications for retinal neovascularization during post-ischemic inflammation. *Graefes Arch. Clin. Exp. Ophthalmol.* **242**, 409–413.

Zhang Y, Hong Y, Bounhar Y, Blacker M, Roucou X, Tounekti O, Vereker E, Bowers WJ, Federoff HJ, Goodyer CG, LeBlanc A (2003) p75 neurotrophin receptor protects primary cultures of human neurons against extracellular amyloid beta peptide cytotoxicity. *J. Neurosci.* **23**, 7385–7394.

Supporting Information

Additional supporting information may be found in the online version of this article:

Data S1 Animal treatment.

Fig. S1 Subretinal injection of Aβ in mice.

Fig. S2 Primers used for qPCR.

Fig. S3 Sequence of cellular events and processes involved in the responses of retina to Aβ.

As a service to our authors and readers, this journal provides supporting information supplied by the authors. Such materials are peer reviewed and may be re-organized for online delivery, but are not copy-edited or typeset. Technical support issues arising from supporting information (other than missing files) should be addressed to the authors.